IEEE Open Journal of
Power Electronics

Received 13 November 2023; revised 6 January 2024 and 22 January 2024; accepted 28 January 2024. Date of publication 31 January 2024; date of current version 1 March 2024. The review of this article was arranged by Associate Editor Al-Thaddeus (OJ GAE) Avestruz.

Digital Object Identifier 10.1109/OJPEL.2024.3360878

Design and Optimization of a Planar Omnidirectional Wireless Power Transfer System for Consumer Electronics

XIPEI YU [1] (Student Member, IEEE), JUNJIE FENG [2] (Member, IEEE), LIYAN ZHU [3] (Member, IEEE), AND QIANG LI [3] (Member, IEEE)

[1]Bradley Department of Electrical and Computer Engineering, Virginia Polytechnic Institute and State University, Blacksburg, VA 24061-0131 USA
[2]Virginia Polytechnic Institute and State University, Blacksburg, VA 24061-0131 USA
[3]Center for Power Electronics Systems, Virginia Tech, Blacksburg, VA 24061-0131 USA

CORRESPONDING AUTHOR: LIYAN ZHU (e-mail: liyanz@vt.edu)

ABSTRACT Recently, omnidirectional wireless power transfer (WPT) has gained increasing popularity due to its capability to charge in arbitrary positions and directions. However, existing solutions still face several challenges, including coupled coils, non-optimized structure, non-uniform magnetic field, and poor misalignment tolerance. This work proposes an omnidirectional WPT system with three fully decoupled coils consisting of one square coil and two perpendicular DD coils. Comprehensive modeling and Pareto optimization for the transmitter coil structure are conducted for improved tolerance to both lateral and angular misalignment. Experimental results are provided to validate the system performance in terms of the output voltage and efficiency under different lateral and angular misalignments. With a 12 V input, the efficiency of the system exhibits a $<$10% variation, ranging from 69% to 78%, with 50 mm misalignment in the x and y axes and a 90-degree angular misalignment. At the same time, the output voltage remains within the range of 11.5 V to 14.5 V.

INDEX TERMS Omnidirectional wireless power transfer, coil modeling, uniform field distribution, coil optimization.

I. INTRODUCTION

Starting from the pioneering work of Nikola Tesla, wireless power transfer (WPT) has received considerable attention, especially in the last two decades due to its ability to transfer power without physical contact. WPT technology is known for numerous benefits, such as electrical isolation, safety, convenience, and adaptability to harsh environments. These benefits make it an attractive choice for a wide range of applications like electric vehicles [1], [2], [3], automatic guided vehicles [4], [5], [6], biomedical implants [7], [8], [9], Internet of Things [10], [11], [12], and consumer electronics [13], [14], [15].

Particularly in the consumer electronics industry, the WPT has gained significant popularity as a convenient solution for battery charging. However, the commonly employed planar structures for transmitter coils pose a strict alignment requirement, as depicted in Fig. 1(a). If the receiver coil is not perfectly aligned with the transmitter coil, the WPT system may not work properly or efficiently. Moreover, for consumer electronics applications like earphones and electronic watches, lateral and angular misalignment is natural as shown in Fig. 1(b). Such misalignment can significantly reduce the magnetic coupling, leading to compromised efficiency and charging experience.

(a) (b)

FIGURE 1. Current practice of wireless charging pad. (a) Fully aligned case. (b) When angular misalignment exists.

Various omnidirectional WPT systems have been proposed to accommodate the different charging positions. In [16], a bowl-shaped WPT system is proposed. However, it utilizes identical currents in transmitter coils, resulting in a fixed magnetic field vector and power transfer direction. Another design proposed in [17] uses a three-orthogonal-coil structure that can generate an omnidirectional magnetic field, but it has limited free-positioning performance due to the poor uniformity of the magnetic field. In [18], a three-coil WPT system is proposed, but it lacks the Y-direction magnetic field. A double three-dimensional (3-D) coil is utilized in [19], but its non-uniform magnetic field leads to extreme degradation when misalignment exists. In [15], a new bowl-shaped structure is proposed, that does realize omnidirectional WPT but its complex structure brings manufacturing challenges.

While planar omnidirectional WPT systems feature simple structures thus facilitating the fabrication and furniture integration, they do not inherently contribute to enhanced performance. For instance, the reticulated structure in [20] still exhibits weak magnetic fields in the y direction and low transfer efficiency. Similarly, the planar structure proposed in [21], which is composed of a metasurface, driver loop, and resonator, has low transfer efficiency and weak magnetic fields in the x and y directions. A crossed dipole coil is analyzed in [22], but due to its sparse coil distribution, its transfer efficiency is low. In [23], a tripolar structure is proposed but its anti-misalignment performance is quite limited. Obviously, the planar structures have benefits in integration compatibility, but optimization in structure design and improvement in anti-misalignment performance are still missing.

From the discussion above, existing planar omnidirectional WPT systems still face challenges such as:

1) Special coil structures are widely applied to extend the charging area coverage. However, in consumer electronics applications, square coils are preferred on the receiver side, which is not compatible with most of the existing solutions. A new transmitter structure that is compatible with consumer receivers is appealing.
2) The design of the most existing structures is based on simulation. However, simulation is time-consuming as many parameter combinations need to be taken into consideration. In order to simplify the design process, analytical models for coil design and optimization are needed.
3) Previous analysis focuses on the realization of a 3-D magnetic field without optimization. This results in uneven magnetic field distribution and poor misalignment tolerance [16], [20], [23]. An optimization process to improve both the lateral and angular misalignments is imperative.

Some coil structures employing the combination of square coil and DD coil have been proposed. However, some emerging problems still exist. The solution is to increase the number of square coils, which will increase the cost. For example, in [24], a quadrupolar coil is proposed. However, the biggest problem is that at 20% x-axis misalignment, it will have a zero-coupling point, which is not practical in real application. In [25], a square coil matrix is used as the transmitter coil and a flux pipe coil is applied as the receiver coil. This coil is cost-intensive and its anti-orientation misalignment performance is limited. For example, in [26], two DD coils are applied as transmitter coils, and two DD coils are applied as the receiver coil. This structure utilizes four DD coils which is cost-intensive. Meanwhile, the anti-misalignment is not mentioned which might be a big issue for the real application. For [27], a DD coil is applied as the transmitter coil while a DD coil is used as the receiver coil. Meanwhile, two square coils are used as the data coil. For this structure, the data coil does not contribute to the power transfer and the mutual inductance decreases sharply versus Z direction misalignment. In [28], one square coil is used as the transmitter coil, and one DD coil is used as the receiver coil, while one square coil and one DD coil are applied as the relay coil. The three-coil structure is complex and according to Table 2 of [28], the mutual inductance decreases by 30% with only 15% diameter misalignment. For [29], the authors investigate the different display possibilities of the DD coil and two square coils, of which the DD coil can be viewed as two rectangular coils. The transmitter coil design is not mentioned at all. From the experimental results, the output voltage decreases by two-thirds at 30% orientation misalignment. At the same time, the receiver coil should be defined by standards like Qi or AirFuel Alliance to increase compatibility rather than self-defined.

To address the aforementioned issues, this paper proposes a planar omnidirectional transmitter that is comprised of two DD coils perpendicular to each other and one square coil to obtain better anti-misalignment performance for a square coil receiver. DD coils are employed to generate the X and Y direction magnetic field while the square coil generates the Z directional field. The planar structure will naturally solve the integration compatibility problem. Modeling and optimization of the proposed structure are also performed to deliver optimal performance.

TABLE 1 Calculation and Simulation Parameters

Symbol	Value	Symbol	Value
s_p	90 mm	s_{s_z}	35 mm
d_p	10 mm	d_{s_z}	1.5 mm
N_{p_z}	4	N_{s_z}	6
L	100 mm	d_a	6 mm
W	90 mm	s_{s_x}	35 mm
d	10 mm	d_{s_x}	1.5 mm
d_b	8 mm	N_{s_x}	6

TABLE 2 Calculation and Simulation Time

Coil	Calculation time	Simulation time
Z coil	0.6 s	295 s
X and Y coil	1.1 s	512 s

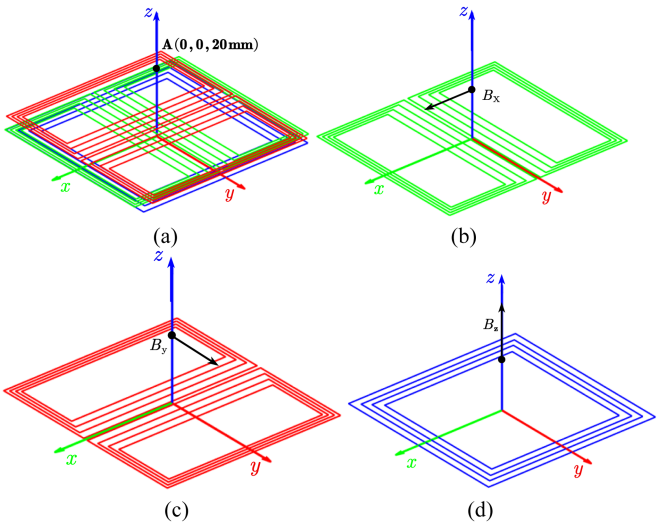

FIGURE 2. Proposed transmitter coil structure. (a) Assembled transmitter coils. (b) X coil. (c) Y coil. (d) Z coil.

The rest of the article is organized as follows: Section II introduces the operation principle of the coil structure. Section III conducts the modeling of the coil structure. In Section IV, the lateral and angular misalignment effects are studied, and the optimal coil parameters are selected by the Pareto front from the multi-objective optimization to obtain a strong and uniform magnetic field. In Section V, simulation results are presented to validate the analytical modeling. Additionally, an experimental prototype is built, and experimental verification is conducted to verify the design. Finally, Section VI concludes this work.

II. PROPOSED PLANAR OMNIDIRECTIONAL WPT SYSTEM

The proposed planar omnidirectional WPT system is illustrated in Fig. 2. The transmitter coil comprises three sets of coils, including one square coil and two DD coils oriented perpendicular to each other. The square Z coil mainly provides the magnetic field in the Z direction while the X and Y DD coils mainly provide the magnetic field in the X and Y directions. The total magnetic field at point $A_1(0, 0, 20$ mm) can be obtained by adding the magnetic field vector in respective directions depicted in (1):

$$\boldsymbol{B}_{\mathbf{total}} = f(i_1)\boldsymbol{B}_{\mathbf{x}} + f(i_2)\boldsymbol{B}_{\mathbf{y}} + f(i_3)\boldsymbol{B}_{\mathbf{z}} \tag{1}$$

The excitation currents in these three transmitter coils are set as:

$$i_1 = I_{\mathrm{m}}\cos(\omega_1 t)\cos(\omega_2 t)\sin(\omega_0 t) \tag{2}$$

$$i_2 = I_{\mathrm{m}}\sin(\omega_1 t)\cos(\omega_2 t)\sin(\omega_0 t) \tag{3}$$

$$i_3 = I_{\mathrm{m}}\sin(\omega_2 t)\sin(\omega_0 t) \tag{4}$$

where $\omega_0{=}2\pi{*}6.78$ MHz, $\omega_1{=}2\pi{*}2.5$ Hz, $\omega_2{=}2\pi{*}50$ Hz. By applying the current specified in (2)–(4) to the utilized coil structure, a 3-D rotating magnetic field can be generated.

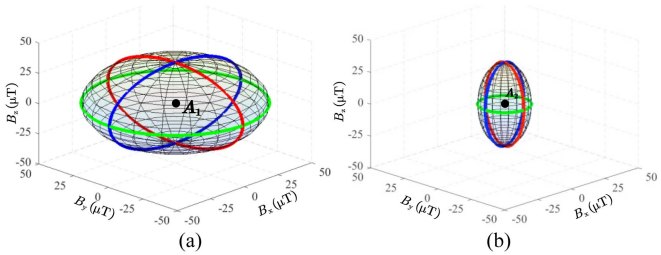

FIGURE 3. Initial magnetic field trajectories: (a) at (0, 0, 20 mm), (b) at (60 mm, 60 mm, 20 mm).

Due to the rotating excitation as depicted in (2)–(4), the flux density at a given position is not a constant but a time-variant vector. By applying current in (2)–(4), the magnetic field vector $\boldsymbol{B}_{\mathrm{total}}$ at different time constants can be derived. Meanwhile, it can be decomposed as $\boldsymbol{B}_{\mathrm{total}}{=}\boldsymbol{B}_{\mathrm{x}}{+}\boldsymbol{B}_{\mathrm{y}}{+}\boldsymbol{B}_{\mathrm{z}}$. Afterward, the combination of B_{x}, B_{y}, and B_{z} can be plotted in Fig. 3, representing the vector trajectories at two example points, $A_1(0, 0, 20$ mm) and $A_2(60$ mm, 60 mm, 20 mm). The field trajectory is on the surface of an ellipsoid. The corresponding envelope curve in X, Y, and Z directions is depicted in red, green, and blue lines. The results confirm that the proposed structure generated an omnidirectional magnetic field. However, it also indicates a non-uniform flux density distribution throughout the entire area, which necessitates the modeling and optimization of the coil parameters.

III. MODELLING OF PLANAR WPT COIL

The square coil and DD coil can be regarded as multiple lines connected in series. Due to the superposition principle, the mutual inductance between transmitter and receiver coils can be represented as the sum of the contribution of each line. The calculation can be derived according to [30]. The assumption is that the self-resonant frequency is at least 2 times larger than the resonant frequency.

When the WPT system operates at the resonant frequency, the coupler efficiency can be calculated as [31]:

$$\eta = \frac{\lambda}{\left(1+\sqrt{1+\lambda}\right)^2}, \lambda = \frac{\omega^2 M^2}{R_p R_s} \tag{5}$$

where M is the mutual inductance, ω is the angular frequency, and R_{p} and R_{s} are the resistance of the coils. According to (5), the coupler efficiency is directly related to the mutual inductance, which should be optimized for efficiency improvement. Prior to that, the mutual inductance should be modeled first.

A. MODELLING OF Z COIL

Fig. 4(a) depicts the schematic of the Z coil with the receiver coil with lateral misalignment. Assuming the transmitter coil has the same spacing, denoted as d_{p}. The turns number of the transmitter coil is N_{p} while that of the receiver coil is N_{s}. The diameter of the outer transmitter coil is denoted as s_{p}. The diameter of the outer receiver coil is denoted as s_{s}. The spacing is denoted as d_{s}. The height of the receiver coil is

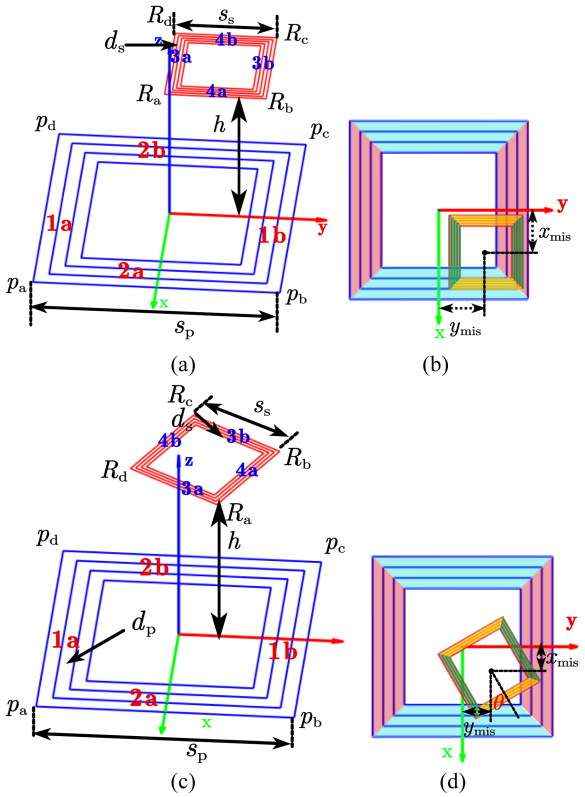

FIGURE 4. Phone charging case with misalignment: (a) the Z coil and the receiver coil with lateral misalignment (b) top view. (c) The Z coil and the receiver coil with lateral and angular misalignment (d) top view.

denoted as h and the center of the receiver coil is denoted as x_{mis} and y_{mis} in Fig. 4(b).

By applying the superposition principle, the mutual inductance between the transmitter and receiver coils can be calculated by:

$$M = \sum_{i=1}^{2} \left(M_{\text{ia(i+2)a}} + M_{\text{ia(i+2)b}} + M_{\text{ib(i+2)a}} + M_{\text{ib(i+2)b}}\right) \tag{6}$$

where $M_{\text{(i+1)a(i+3)a}}$ represents the mutual inductance between part (i+1)a and part (i+3)a shown in Fig. 4(a). The definition for other parts is similar. For example, M_{1a3a} can be calculated as:

$$M_{\text{1a3a}} = \sum_{k=0}^{N_{\text{p}}} \sum_{i=1}^{N_{\text{s}}} M(s_{\text{p}} - 2kd_{\text{p}}, s_{\text{s}} - 2id_{\text{s}}, d_{\text{z\_1a,k\_3a\_i}}, \Delta_{\text{z\_1a,k\_3a\_i}}) \tag{7}$$

where

$$d_{\text{z\_1a,k\_3a\_i}} = \sqrt{\left(\frac{s_{\text{p}}}{2} - \frac{s_{\text{s}}}{2} + y_{\text{center}} - kd_{\text{p}} + id_{\text{s}}\right)^2 + h^2}$$

$$\Delta_{\text{z\_1a,k\_3a\_i}} = -\frac{s_{\text{p}}}{2} + \frac{s_{\text{s}}}{2} + x_{\text{center}} + id_{\text{s}} + kd_{\text{p}} \tag{8}$$

When the angular misalignment exists, the schematic of Z coil with a receiver coil is shown in Fig. 4(c). θ is defined as the counterclockwise angle in Fig. 4(d). The parameter definition is

$$M = \sum_{k=1}^{2} \sum_{i=1}^{2} \left(M_{\text{ia(k+2)a}} + M_{\text{ia(k+2)b}} + M_{\text{ib(k+2)a}} + M_{\text{ib(k+2)b}}\right) \tag{9}$$

For instance, M_{1a3a} can be calculated by:

$$M_{\text{1a3a}} = \sum_{k=0}^{N_{\text{p}}} \sum_{i=0}^{N_{\text{s}}} M(s_{\text{s}} - 2id_{\text{s}}, s_{\text{p}} - 2kd_{\text{p}}, P_{\text{a}}R_{\text{d}}, P_{\text{a}}R_{\text{a}}, P_{\text{d}}R_{\text{d}}, P_{\text{d}}R_{\text{a}}) \tag{10}$$

$$\begin{aligned} P_{\text{a}} &= \left(\frac{s_{\text{p}}}{2} - kd_{\text{p}}, -\frac{s_{\text{p}}}{2} + kd_{\text{p}}, 0\right), \\ P_{\text{d}} &= \left(-\frac{s_{\text{p}}}{2} + kd_{\text{p}}, -\frac{s_{\text{p}}}{2} + kd_{\text{p}}, 0\right) \\ R_{\text{a}} &= \left(\sqrt{2}\left(\frac{s_{\text{s}}}{2} - id_{\text{s}}\right)\cos\left(\frac{\pi}{4} - \theta\right) + x_{\text{center}}, \right. \\ &\quad \left. \sqrt{2}\left(\frac{s_{\text{s}}}{2} - id_{\text{s}}\right)\sin\left(\frac{\pi}{4} - \theta\right) + y_{\text{center}}, h\right) \\ R_{\text{d}} &= \left(\sqrt{2}\left(\frac{s_{\text{s}}}{2} - id_{\text{s}}\right)\sin\left(\frac{\pi}{4} - \theta\right) + x_{\text{center}}, \right. \\ &\quad \left. -\sqrt{2}\left(\frac{s_{\text{s}}}{2} - id_{\text{s}}\right)\cos\left(\frac{\pi}{4} - \theta\right) + y_{\text{center}}, h\right) \end{aligned} \tag{11}$$

B. MODELLING OF X AND Y COIL

X coil with a receiver coil with lateral misalignment is depicted in Fig. 5(a). X coil has two rectangular coils connected in series in the opposite direction, of which the length and width of the rectangular coil are $2L$ and W, respectively. The distance between these two rectangular coils is defined as $2d$ and d_{a} and d_{b} are denoted as the outer and inner spaces of the rectangular coil. The turn number of the transmitter coil is N_{p} while the turn number of the receiver coil is N_{s}. The parameter definition of a receiver coil is similar to that of the Z coil case.

The mutual inductance between the X coil and the receiver coil can be modeled as:

$$M = \sum_{k=1}^{2} \sum_{i=1}^{2} \left(M_{\text{ia(k+2)a}} + M_{\text{ia(k+2)b}} + M_{\text{ib(k+2)a}} + M_{\text{ib(k+2)b}}\right) \tag{12}$$

where M_{1a5a} can be given in (13) and (14): The other parameter calculation can be calculated similarly to M_{1a5a}.

$$M_{\text{1a5a}} = \sum_{k=0}^{N_{\text{p}}} \sum_{i=0}^{N_{\text{s}}} M(2L - 2kd_{\text{a}}, s_{\text{s}} - 2id_{\text{s}}, d_{\text{x\_1a,k\_5a\_i}}, \Delta_{\text{x\_1a,k\_5a\_i}}) \tag{13}$$

$$d_{\text{x\_1a,k\_5a\_i}} = \sqrt{(d + W - x_{\text{center}} - kd_{\text{a}})^2 + (h + id_{\text{s}})^2}$$

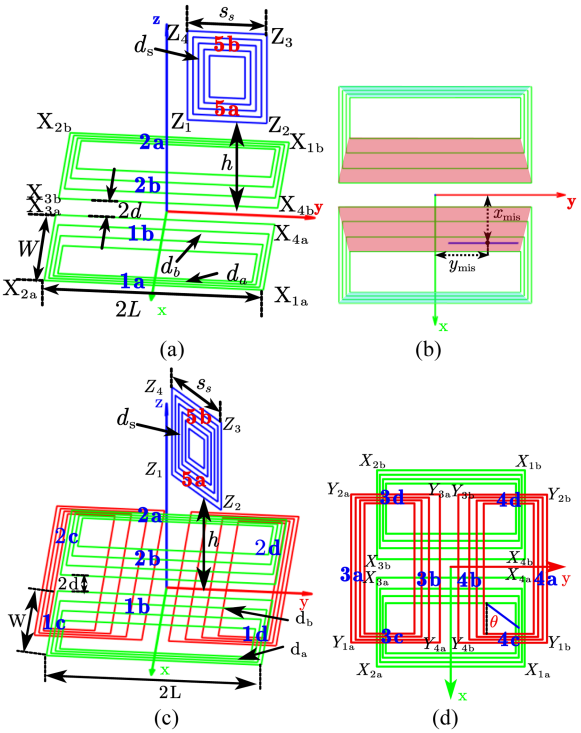

FIGURE 5. Watch charging case with misalignment: (a) the X coil with a receiver coil with lateral misalignment (b) top view. (c) The X coil with receiver coil with lateral and angular misalignment (d) top view.

$$\Delta_{\mathrm{x\_1a,k\_5a\_i}} = -\frac{s_\mathrm{s}}{2} + y_\mathrm{center} - L + id_\mathrm{s} + kd_\mathrm{a} \tag{14}$$

Similar to the phone charging case, angular misalignment also exists between the receiver and X-Y coils in the watch charging case. But different from the phone charging case, when angular misalignment exists, both X and Y coils contribute to the receiver coil, as shown in Fig. 5(c). Under this circumstance, M can be modeled as:

$$M = \sum_{k=1}^{4} \begin{pmatrix} M_\mathrm{ia5a} + M_\mathrm{ib5a} + M_\mathrm{ic5a} + M_\mathrm{id5a} \\ + M_\mathrm{ia5b} + M_\mathrm{ib5b} + M_\mathrm{ic5b} + M_\mathrm{id5b} \end{pmatrix} \tag{15}$$

where M_{1a5a} can be given as:

$$M_{1a5a} = \sum_{k=0}^{N_\mathrm{p}} \sum_{i=0}^{N_\mathrm{s}} M(s_\mathrm{s} - 2id_\mathrm{s}, 2L - 2kd_\mathrm{a}, X_\mathrm{1a}Z_2, X_\mathrm{1a}Z_1, X_\mathrm{2a}Z_1, X_\mathrm{2a}Z_2) \tag{16}$$

$$X_\mathrm{1a} = (d + W - kd_\mathrm{a}, L - kd_\mathrm{a}, 0)$$

$$X_\mathrm{2a} = (d + W - kd_\mathrm{a}, -L + kd_\mathrm{a}, 0)$$

$$Z_1 = \left(\frac{s_\mathrm{s} - id_\mathrm{s}}{2} \sin\theta + x_\mathrm{center}, -\frac{s_\mathrm{s} - id_\mathrm{s}}{2} \cos\theta + y_\mathrm{center}, h + id_\mathrm{s} \right)$$

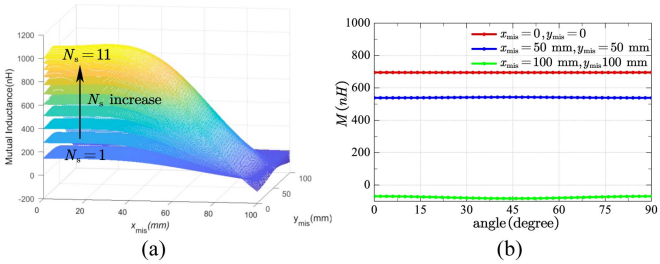

FIGURE 6. Mutual inductance between the Z coil and the receiver coil with different N_s: (a) versus lateral misalignment (b) versus angular misalignment.

$$Z_2 = \left(-\frac{s_\mathrm{s} - id_\mathrm{s}}{2} \sin\theta + x_\mathrm{center}, \frac{s_\mathrm{s} - id_\mathrm{s}}{2} \cos\theta + y_\mathrm{center}, h + id_\mathrm{s} \right) \tag{17}$$

Similarly, other mutual inductance can be obtained via the calculation process of M_{1a5a}.

IV. COIL OPTIMIZATION OF PLANAR WPT COIL

As illustrated in Fig. 3, the magnetic field distribution of the charging system is not uniform, which results in lower efficiency and reduces the charging power at certain positions of the receiver. Therefore, to address this issue, coil optimization is necessary to achieve a consistent and strong magnetic field throughout the entire charging area. For the optimization process, all three coils should be conducted, but due to the symmetry, only X and Z coils are shown here.

A. N_S AND ANGULAR MISALIGNMENT EFFECT ON Z COIL

For mobile phone applications, a receiver with s_s= 70 mm and d_s= 1.5 mm is used. The resonant frequency is selected at 6.78 MHz, which is recommended by the AirFuel Alliance [32], [33]. In order to cater to the Qi standard at the same time [34], [35], [36], the N_s effect on the coupling should be studied first. Here, s_p= 90 mm, d_p= 10 mm, and N_p= 4 are selected as initial parameters. The mutual inductance with different N_s versus lateral misalignment is shown in Fig. 6(a). It can be observed that the trend under different N_s remains similar. This implies that the selection of N_s won't affect the mutual inductance distribution throughout the whole area. Therefore, optimization can be conducted for any specific N_s. In this work, N_s= 6 is selected to accommodate the coil size.

Angular misalignment is important for omnidirectional applications. For the phone charging case, the mutual inductance can be calculated according to (6)–(8) when the angular misalignment exists. For instance, when s_p= 90 mm, d_p= 10 mm, and N_p= 4, mutual inductance versus the angular misalignment is plotted in Fig. 6(b). The results demonstrate that the mutual inductance is merely affected by the angular misalignment due to the introduction of the square coil on the transmitter side. Therefore, for the phone charging case, the optimization process can be conducted without considering the angular misalignment.

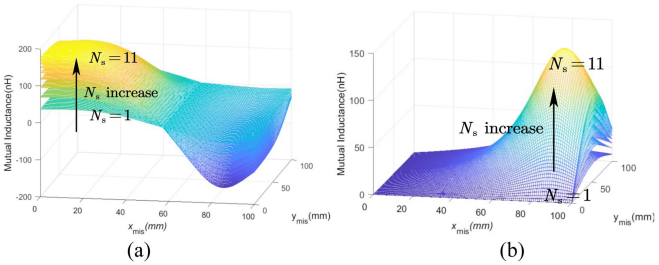

FIGURE 7. Mutual inductance with different N_s versus lateral misalignment: (a) between X coil and a receiver, (b) between Y coil and receiver.

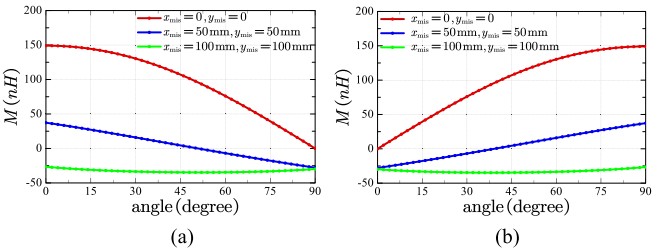

FIGURE 8. Mutual inductance versus angular misalignment: (a) X coil and a receiver coil, (b) mutual inductance of Y coil and a receiver coil.

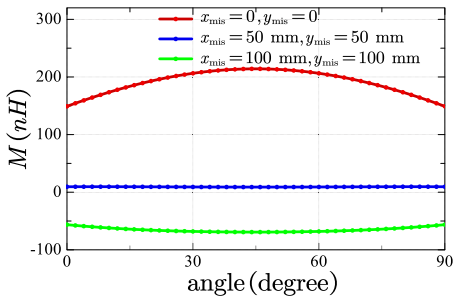

FIGURE 9. Mutual inductance of X and Y coil and a receiver coil versus angular misalignment of several points.

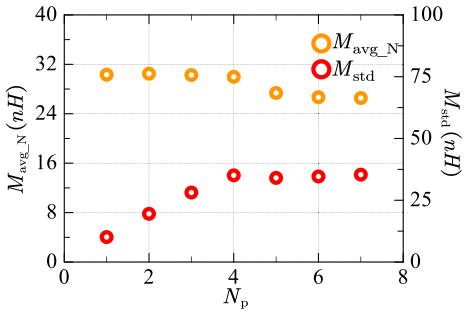

FIGURE 10. M_{avg} and M_{std} under different N_p.

B. N_S AND ANGULAR MISALIGNMENT EFFECT ON X AND Y COIL

For X and Y coils, a receiver with s_s= 38 mm and d_s= 1.5 mm is adopted to emulate the receiver coil of an electronic watch. Similarly, the N_s effect on the coupling should be investigated first. Here, the dimensions of L= 90 mm, W= 80 mm, d= 10 mm, d_a= 4 mm, d_b= 10 mm, and N_p=4 are selected as initial parameters. The results for X and Y coils are illustrated in Fig. 7. It is observed that the trend under different N_s remains similar. This aligns with the phone charging case, and N_s=6 is selected as the same.

Similarly, it is necessary to consider the effect of angular misalignment. For the X coil, mutual inductance versus angular misalignment of several points can be plotted in Fig. 8(a) and (b). It is evident that angular misalignment will significantly affect the mutual inductance and it cannot be ignored. Fortunately, when the mutual inductance between the X coil and the receiver coil is suffering from angular misalignment, the Y coil compensates. As a result, the overall mutual inductance remains relatively consistent even with angular misalignment, as illustrated in Fig. 9. Therefore, X and Y coils should be considered as a whole, and the angular misalignment can be ignored to focus the further optimization on lateral misalignment.

C. OPTIMIZATION OF X AND Y COILS FOR WATCH CHARGING

For X and Y coils, a receiver coil with s_s= 38 mm, d_s= 1.5 mm, and N_s= 6 is selected to emulate the receiver of an electronic watch.

Here the whole charging area is defined as a square area with a 200 mm diameter. Due to the symmetry of magnetic field distribution, only the first quadrant is considered. Here 11∗11 characteristic points of the first quadrant are selected, with a step of 10 mm, M_{avg} represents the average value of these points while M_{std} represents the standard deviation of these points. The specific equations of M_{avg} and M_{std} derivation can be written as:

$$M_{avg} = \frac{1}{121}\sum_{j=1}^{11}\sum_{i=1}^{11} M_{ij} \tag{18}$$

$$M_{std} = \sqrt{\sum_{j=1}^{11}\sum_{i=1}^{11}\left(M_{ij} - M_{avg}\right)^2} \tag{19}$$

According to Fig. 3, the magnetic field distribution is not uniform. To achieve high M_{avg} and low M_{std} for the whole charging area, the magnetic field strength and uniformity need to be optimized.

Firstly, N_p should be selected. d_a= 10 mm, d_b= 4 mm with even coil segment line distribution is considered as the initial setting. The relation between the N_p and the M_{avg} and M_{std} is depicted in Fig. 10. The results show that when $N_p \leq 4$, the M_{std} decreases sharply, which indicates uneven field distribution cases. When $N_p \geq 4$, M_{avg} increases while M_{std} is stable. However, if keep increasing the N_p, the average mutual inductance contributed by each turn M_{avg_N} will decrease, which implies a low charging area utilization. Therefore, the optimal turn number N_p should be identified as 4.

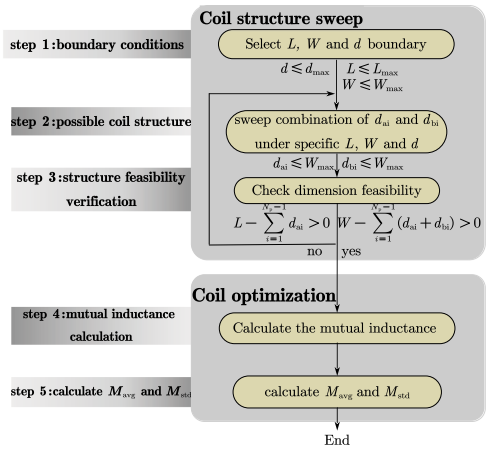

FIGURE 11. Multi-objective coil optimization process of X and Y coil.

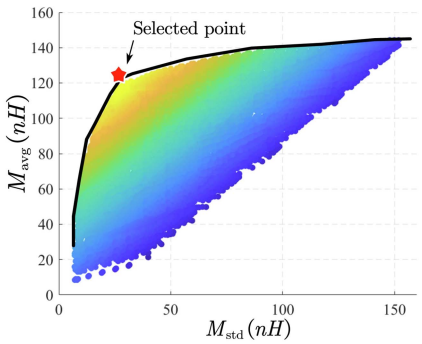

FIGURE 12. Relationship between M_{avg} and M_{std} when N_p= 4.

Once N_p is selected as 4, the further optimization objectives are to maximize M_{avg} while minimizing M_{std} over the entire area by optimizing the coil spacing. With given s_p, first all the combinations of d_{ai} and d_{bi} should be derived. The only limitation is that the length of the inner coil should be larger than 0. By obtaining all the possible combinations, then the mutual inductance across all the characteristic points in the first quadrant can be derived and M_{avg} and M_{std} values can be obtained accordingly by (18) and (19). Afterwards, the multi-objective optimization is conducted and the flowchart of this optimization is shown in Fig. 11.

Following this flowchart, the corresponding Pareto Front can be plotted. The optimal operating point is identified, which is denoted by a red star in Fig. 12. Specifically, the optimal value is L= 100 mm, W= 200 mm, d= 16 mm, d_{b1}= 4 mm, d_{b2}= 18 mm, and d_{b3}= 20 mm.

D. OPTIMIZATION OF Z COILS FOR PHONE CHARGING

For Z coil, the common circumstance is to charge the mobile phone flat on the charging pad. A receiver coil with s_s= 70 mm, d_s= 1.5 mm, and N_s= 6 is chosen to emulate the mobile phone receiver as discussed previously.

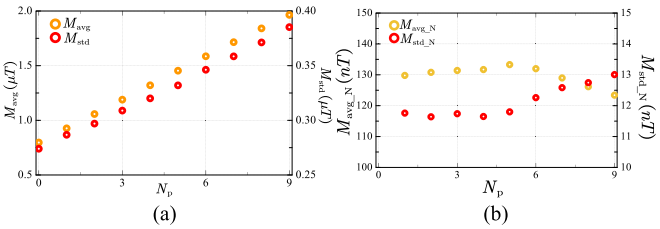

FIGURE 13. (a) M_{avg} and M_{std} verse different N_p. (b) M_{avg_N} and M_{std_N} verse different N_p.

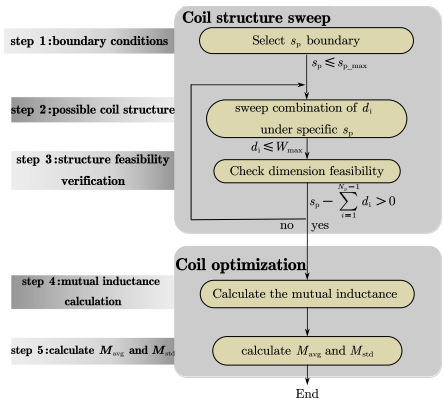

FIGURE 14. Multi-objective coil optimization process of Z coil.

Unlike the X and Y coil case, the Z coil contributes little to the X and Y magnetic field, However, due to the planar structure, X and Y coils do make contributions to the Z magnetic field. Although this contribution is trivial at the center point [37], it becomes significant when there is lateral misalignment. This mechanism beneficially compensates for the mutual inductance reduction between the receiver and Z coil when lateral misalignment happens. When conducting the optimization of the Z coil, this factor should be considered.

Similarly, N_p should be selected first. The relation between the N_p and the M_{avg} and M_{std} is plotted in Fig. 13(a). According to Fig. 13(a), M_{avg} and M_{std} increase almost linearly with the increase of N_p which means it is hard to select the optimal N_p. In order to select the optimal N_p, further analysis should be conducted. Similar to the analysis conducted for the X and Y coils, the average contribution of each turn should be considered. Therefore, M_{avg_N} and M_{std_N} should be the criteria and are plotted in Fig. 13(b). From M_{avg_N} point of view, when $N_p \leq 5$, M_{avg_N} is almost constant, and when $N_p \geq 5$, M_{avg_N} decreases slightly. From M_{std_N} point of view, when $N_p \leq 5$, M_{std_N} is almost constant, and when $N_p \geq 5$, M_{std_N} increases slightly. In all, N_p= 5 is the optimal point.

Different from X and Y coils, the Z coil only has a single parameter d, rather than d_a and d_b for X and Y coils. Similarly, to achieve high M_{avg} and small M_{std}, multi-objective optimization is conducted. The flowchart is shown in Fig. 14, and the corresponding Pareto Front is plotted in Fig. 15, with

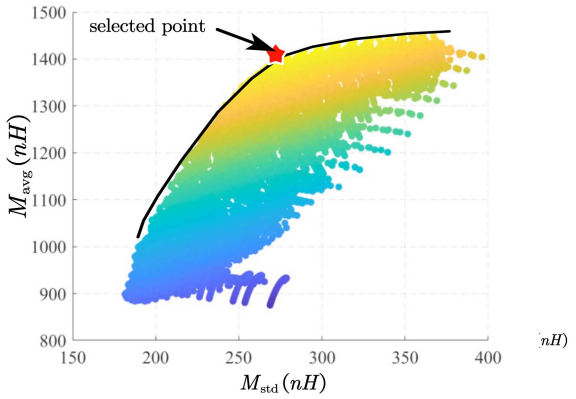

FIGURE 15. Relationship between M_{avg} and M_{std} when $N_p = 5$.

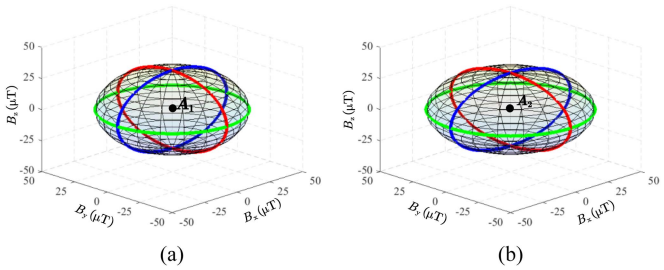

FIGURE 16. Magnetic field trajectories after optimization: (a) at (0, 0, 20 mm), (b) at (60 mm, 60 mm, 20 mm).

optimal parameters as $s_p = 135$ mm, $d_{p1} = 9$ mm, $d_{p2} = 9$ mm, $d_{p3} = 9$ mm, $d_{p4} = 38$ mm.

With the optimal coil parameters, the optimized magnetic vector trajectories are given in Fig. 16. Compared to the initial one shown in Fig. 3, a clear improvement in anti-misalignment performance is exhibited. More evidence of the improved filed distribution will be illustrated in the next section from the output voltage point of view.

V. SIMULATION AND EXPERIMENTAL VERIFICATION

During the modeling process, the displacement current is not considered and the parasitic capacitance is ignored. In order to verify the assumption, the impedance of the coils is swept by the Keysight E4990A Impedance Analyzer as plotted in Fig. 17. The results show a self-resonant frequency over 32 MHz, which is five times higher than the resonant frequency and validated the assumption.

A. VERIFICATION OF PROPOSED MODELLING METHODS

To verify the accuracy of the proposed analytical model, the 3-D FEA simulation is conducted with the parameters in Table 1. For the phone charging case scenario as discussed in Fig. 4(a), the comparison of calculated and simulated mutual inductance with misalignments is plotted in Fig. 18, and the watch charging case is given in Fig. 19.

The comparison shows a less than 1% calculation error with both lateral and angular misalignments. Particularly, the

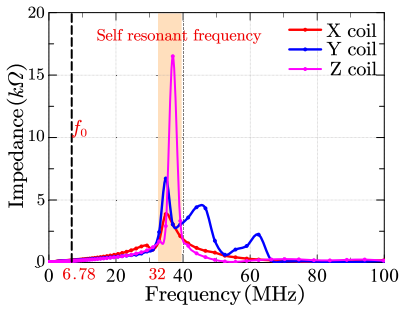

FIGURE 17. Impedance against frequency for the proposed coils. .

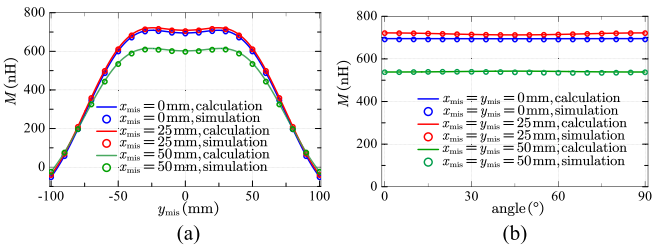

FIGURE 18. Mutual inductance between receiver and Z coil: (a) lateral misalignment; (b) lateral and angular misalignment.

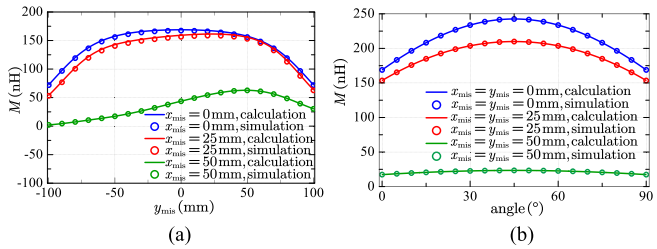

FIGURE 19. Mutual inductance between receiver and X-Y coils: (a) lateral misalignment; (b) lateral and angular misalignment.

results confirm again that the angular misalignment barely affects the mutual inductance value, which aligns with the conclusion made in Section III. In addition, the calculation and Ansys simulation time are recorded in Table 2. Thanks to the analytical model, the calculation shows a much faster calculation speed, which made the parametric optimization possible.

B. HARDWARE SETUP

To verify the feasibility of the proposed WPT system, the omnidirectional WPT prototype is constructed as shown in Fig. 20(a). The LCCL-LC resonant converter is adopted as shown in Fig. 20(b) [14]. The experiment setup consisted of a DC source, three half-bridge inverters, three LCC compensation networks, three sets of transmitter coils, one receiver, series resonant networks, and a load. The system is powered by the Agilent E3631A DC power source with a 12 V input

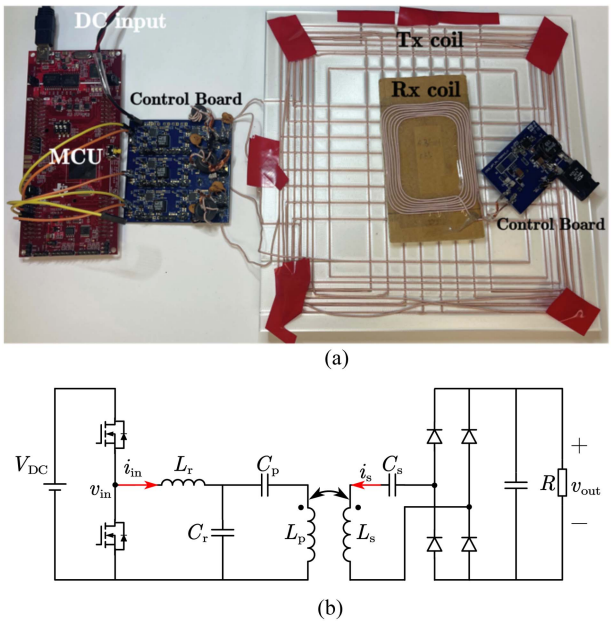

FIGURE 20. (a) Experimental prototype. (b) Circuit diagram of LCCL-LC resonant converter.

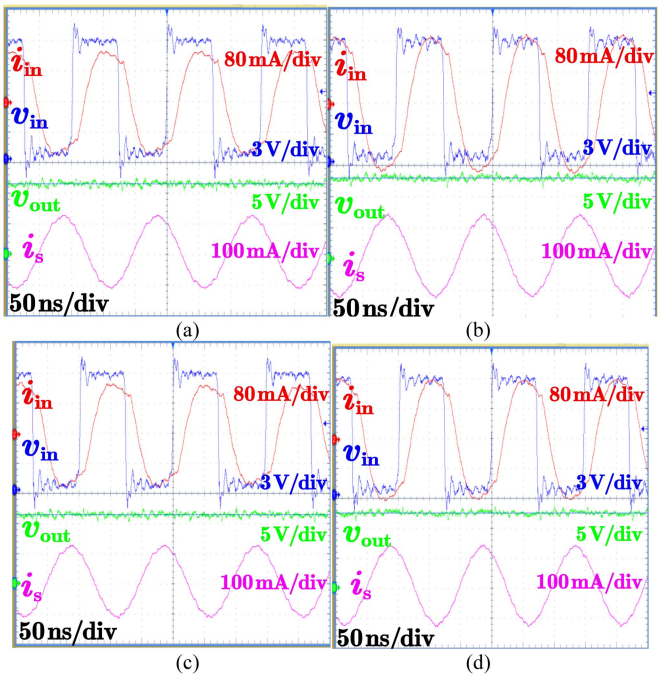

FIGURE 21. Steady-state waveform of phone charging case: (a) at point (0, 0) (b) at point (50 mm, 50 mm) (c) at point (0, 0) with a 45-degree angular misalignment (d) at point (50 mm, 50 mm) with a 45-degree angular misalignment.

TABLE 3 Specifications of WPT System

Specifications	Symbol	Value
X coil self-inductance	L_{p_x}	6.58 uH
Y coil self-inductance	L_{p_y}	6.58 uH
Z coil self-inductance	L_{p_z}	4.91 uH
Mobile phone receiver coil self-inductance	L_{s_m}	3.383 uH
Electronic watch receiver coil self-inductance	L_{s_w}	1.863 uH
Output Capacitor	C_o	4.7 uF
Output resistance	R_o	240 Ω
Compensation inductor for X, Y, and Z coil	L_{r_x}, L_{r_y}, L_{r_z}	1.197 uH, 1.227 uH, 1.178 uH
Compensation capacitor for X, Y, and Z coil	C_{r_x},C_{r_y},C_{r_z}	541 nF, 571 nF,581 nF
Compensation capacitor for X, Y, and Z coil	C_{p_x},C_{p_y},C_{p_z}	46 nF, 113 nF, 112 nF
Mobile phone and watch receiver coil self-inductance	L_{s_m}, L_{s_w}	3.383 uH, 1.863 uH
Mobile phone and watch receiver coil Compensation capacitor	C_{s_m}, C_{s_w}	181pF, 295 pF

voltage. The parameters of the resonant tank are shown in Table 3.

The inductance value of the coils and passive components are measured with the Keysight E4990A Impedance Analyzer as listed in Table 3. To control the coil geometry accurately, the Ultimake S5 3D printer is adopted to print the coil periphery. Here the coil is fabricated by Litz wire and it consists of 450 strands of AWG 48 wires. The Litz wire is fitted into the coil periphery.

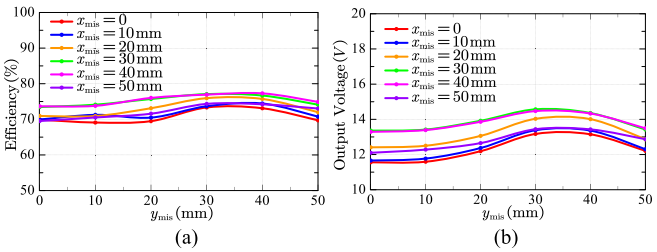

FIGURE 22. Measured results of phone charging case with lateral misalignment (a) efficiency test (b) output voltage.

C. TESTS FOR PHONE CHARGING

For verification of phone charging anti-misalignment performance, the Z coil is independently excited. The waveform of input and output voltage and current at points (0,0) and (50 mm,50 mm) are shown in Fig. 21(a) and (b), and (c) and (d) shows the cases with angular misalignment.

The transfer efficiency and output voltage with different misalignments are measured. As the transmitter coil structure is symmetric, only the misalignment in the first quarter is considered. When there is only lateral misalignment, Fig. 22 shows an efficiency range from 69%-78%, and the output voltage ranges from 11.5 V to 14.5 V, which exhibits a good anti-lateral misalignment performance. When the angular misalignment is considered, the efficiency and output voltage at x_{mis}=y_{mis}=0 mm–50 mm are measured as plotted in Fig. 23. As shown in the figure, the efficiency remained in

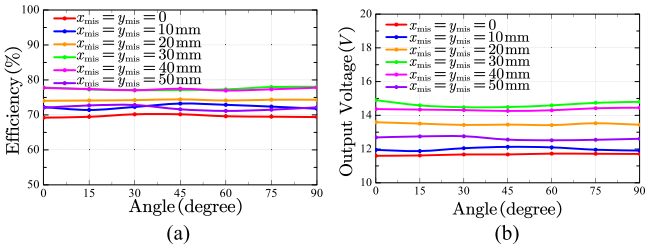

FIGURE 23. Measured results of phone charging case with lateral and angular misalignment (a) efficiency test (b) output voltage.

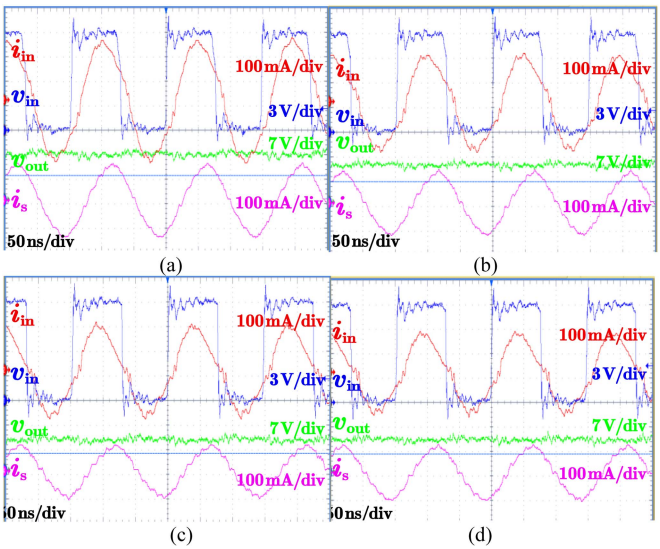

FIGURE 24. Steady-state waveform of watch charging case: (a) at point (0, 0), (b) at point (50 mm, 50 mm), (c) at point (0, 0), and (d) at point (50 mm, 50 mm) with a 30-degree angular misalignment.

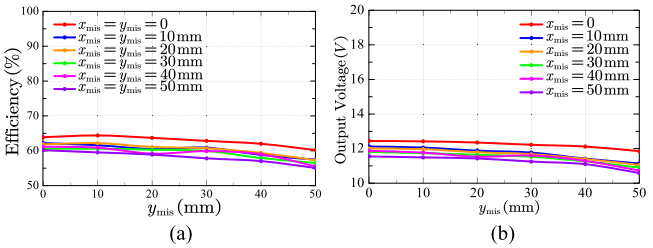

FIGURE 25. Measured results with X coil excited under the misalignment in *x* and *y* orientation (a) efficiency test (b) output voltage.

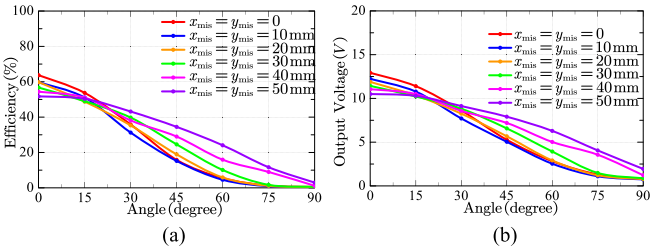

FIGURE 26. Measured results with X coil excited under misalignment in *x* and *y* against the angular misalignment (a) efficiency test (b) output voltage.

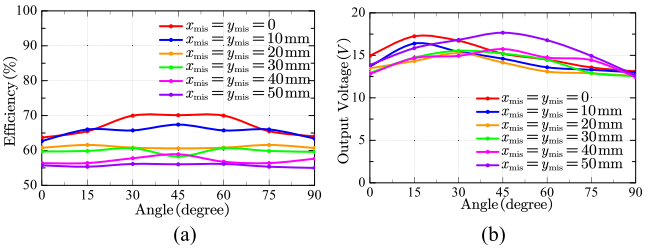

FIGURE 27. Measured results with both X and Y coils excited under lateral and angular misalignment (a) efficiency test (b) output voltage.

the range of 69%-78%, and the output voltage keeps high from 11.5 V to 14.5 V. The results show a good anti-angular misalignment performance, which is consistent with the analysis in Section III.

D. MISALIGNMENT TESTS FOR WATCH CHARGING

For electronic watch applications, the X and Y coils are excited separately, and a square coil with s_s= 38 mm, d_s= 1.5 mm, and N_s= 6 is used as the receiver for electronic watch. Typically, electronic watch users place their watches in a vertical position on the charging pad, as illustrated in Fig. 1(b). As a result, the experiment considers the receiver coil in a vertical position. To account for the thickness of both the electronic watch and charging pad, the height h is set at 10 mm.

The waveform of input and output voltage and current under positions (0,0) and (50 mm,50 mm) when the X coil is excited is shown in Fig. 24(a) and (b). It is observed that the input voltage and current remain stable even under misalignment. The waveform under 30-degree angular misalignment is depicted in Fig. 24(c) and (d).

The transfer efficiency and output voltage at different positions are measured as plotted in Fig. 25. The efficiency ranges from 55% to 65% and the output voltage is constrained from 10.5 V to 12.5 V. At x_{mis}=y_{mis}=0 mm–50 mm with angular misalignment as shown in Fig. 26, the efficiency drops sharply when only X or Y coils are separately excited. It is aligned with the previous analysis. However, when both the X and Y coils work together to counteract angular misalignment, the system performance stays decent, as evidenced in Fig. 27. The stable efficiencies and output voltage validate the previous analysis and optimization.

E. COMPARISON WITH OTHER OMNIDIRECTIONAL WPT SYSTEMS

The comparison with the state-of-the-art omnidirectional WPT system is depicted in Table 4 Compared with the three-dimensional structure like [15], [16], [19], the planar structure is easy to gain compatibility with the home furniture.

As for the anti-misalignment performance, first the anti-orientation misalignment is discussed. In most literature, they

TABLE 4 Comparison With Recent Omnidirectional WPT Systems

Paper	Tx/Rx coil Structure	Compatibility with furniture	Coil structure complexity	Omnidirectional capability with phone	Omnidirectional capability with watch	Optimization process	Anti-lateral misalignment	Anti-angular misalignment	Power and efficiency
[15]	3D/3D	No	Complex	Yes	Yes	Yes	Few	Yes	2 W,60%
[16]	3D/2D	No	Complex	Yes	Yes	No	Few	Few	2 W,40%
[18]	2D/2D	Yes	Simple	Yes	Few	No	Few	Few	0.8 W,14%
[19]	3D/2D	No	Complex	Yes	Few	No	Few	Few	50 W, 50%
[20]	2D/3D	Yes	Complex	Yes	Yes	Yes	Few	Few	1.57 W, 3.12%
[21]	2D/2D	Yes	Complex	Yes	Few	No	Few	Few	1 W,40%
[22]	2D/2D	Yes	Simple	Yes	Few	No	Few	Few	100 W, 33.6%
[24]	2D/2D	Yes	Simple	Yes	Few	No	Few	Few	500W,60%
[25]	2D/2D	Yes	Complex	Yes	Few	No	Yes	Few	350W,65%
[26]	2D/2D	Yes	Complex	Yes	Few	No	Few	Few	10W,40%
[27]	2D/2D	Yes	Simple	Yes	Few	No	Few	Few	5kW,87%
[28]	2D/2D	Yes	Complex	Yes	Few	No	Few	Few	320W, 72%
[29]	2D/2D	Yes	Simple	Yes	Few	No	Few	Few	400W,70%
[38]	2D/2D	Yes	Complex	Yes	Few	No	Few	Few	70W,50%
This work	2D/2D	Yes	Simple	Yes	Yes	Yes	Yes	Yes	2W,78%

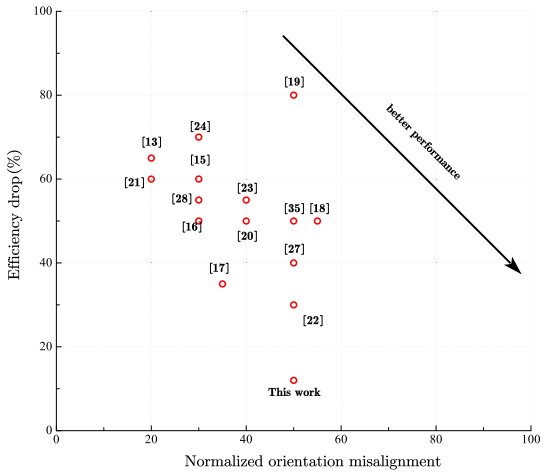

FIGURE 28. Efficiency drop versus normalized orientation misalignment.

fail to mention the anti-misalignment but the efficiency under misalignment is measured. In this case, the efficiency drop at the maximum orientation misalignment can be plotted in Fig. 28. What is desired is stable charging in the whole area, in other words, a low efficiency drop at high normalized orientation misalignment is pursued. According to Fig. 28, this work lies in the bottom right corner, which means this WPT system can achieve low-efficiency drop at large normalized orientation misalignment thanks to the optimization process.

For the angular misalignment, few works are considering this part except for [15]. Although it accounts for this part, its coil structure is very complicated, which means high manufacturing difficulty. Meanwhile, its three-dimensional structure is hard to integrate into the home furniture.

If all the aspects are taken into account, for our proposed coil structure, besides the inherent advantage that easy to integrate with home furniture brought by its planar structure, it can achieve omnidirectional charging while having good anti-orientation misalignment and anti-angular misalignment performance with low-cost and low manufacturing difficulty.

VI. CONCLUSION

This paper proposes a planar omnidirectional WPT system. The modeling process is conducted for the coil structure and its N_s, lateral, and angular misalignment effects are studied. Furthermore, optimization is conducted on the coil structure to achieve free positioning performance. Finally, a 6.78 MHz omnidirectional prototype is built for tests of mobile phone and electronic watch charging cases. Results show an efficiency range of 69%-78% efficiency for the phone charging case and an efficiency range of 55%-65% for the electronic watch charging case. When compared with the state-of-art research in Table 4, the proposed solution presents good anti-lateral and anti-angular misalignment performance on the premise of compatibility with furniture and simplicity in structure, which offers a fundamental and convenient solution for future 3-D omnidirectional wireless charging applications.

REFERENCES

[1] M. Wu et al., "A compact coupler with integrated multiple decoupled coils for wireless power transfer system and its anti-misalignment control," *IEEE Trans. Power Electron.*, vol. 37, no. 10, pp. 12814–12827, Oct. 2022, doi: 10.1109/TPEL.2022.3166888.

[2] M. Wu et al., "Modeling of litz-wire DD coil with ferrite core for wireless power transfer system," *IEEE Trans. Power Electron.*, vol. 38, no. 5, pp. 6653–6669, May 2023, doi: 10.1109/TPEL.2022.3222228.

[3] M. Wu et al., "A dual-sided control strategy based on mode switching for efficiency optimization in wireless power transfer system," *IEEE Trans. Power Electron.*, vol. 36, no. 8, pp. 8835–8848, Aug. 2021, doi: 10.1109/TPEL.2021.3055963.

[4] C. Zhu et al., "Analysis and design of cost-effective WPT systems with dual independently regulatable outputs for automatic guided vehicles," *IEEE Trans. Power Electron.*, vol. 36, no. 6, pp. 6183–6187, Jun. 2021, doi: 10.1109/TPEL.2020.3036353.

[5] Y. Jiang, L. Wang, J. Fang, R. Li, R. Han, and Y. Wang, "A high-efficiency ZVS wireless power transfer system for electric vehicle charging withvariable angle phase shift control," *IEEE J. Emerg. Sel. Topics Power Electron.*, vol. 9, no. 2, pp. 2356–2372, Apr. 2021, doi: 10.1109/JESTPE.2020.2984575.

[6] Y. Wu, H. Yuan, R. Zhang, A. Yang, X. Wang, and M. Rong, "Low-frequency wireless power transfer via rotating permanent magnets," *IEEE Trans. Ind. Electron.*, vol. 69, no. 10, pp. 10656–10665, Oct. 2022, doi: 10.1109/TIE.2022.3158010.

[7] A. K. RamRakhyani, S. Mirabbasi, and M. Chiao, "Design and optimization of resonance-based efficient wireless power delivery systems for biomedical implants," *IEEE Trans. Biomed. Circuits Syst.*, vol. 5, no. 1, pp. 48–63, Feb. 2011, doi: 10.1109/TBCAS.2010.2072782.

[8] K. Agarwal, R. Jegadeesan, Y.-X. Guo, and N. V. Thakor, "Wireless power transfer strategies for implantable bioelectronics," *IEEE Rev. Biomed. Eng.*, vol. 10, pp. 136–161, 2017, doi: 10.1109/RBME.2017.2683520.

[9] Q. Chen, S. C. Wong, C. K. Tse, and X. Ruan, "Analysis, design, and control of a transcutaneous power regulator for artificial hearts," *IEEE Trans. Biomed. Circuits Syst.*, vol. 3, no. 1, pp. 23–31, Feb. 2009, doi: 10.1109/TBCAS.2008.2006492.

[10] Z. Chu, F. Zhou, Z. Zhu, R. Q. Hu, and P. Xiao, "Wireless powered sensor networks for Internet of Things: Maximum throughput and optimal power allocation," *IEEE Internet Things J.*, vol. 5, no. 1, pp. 310–321, Feb. 2018, doi: 10.1109/JIOT.2017.2782367.

[11] K. W. Choi, A. A. Aziz, D. Setiawan, N. M. Tran, L. Ginting, and D. I. Kim, "Distributed wireless power transfer system for Internet of Things devices," *IEEE Internet Things J.*, vol. 5, no. 4, pp. 2657–2671, Aug. 2018, doi: 10.1109/JIOT.2018.2790578.

[12] T. D. Ponnimbaduge Perera, D. N. K. Jayakody, S. K. Sharma, S. Chatzinotas, and J. Li, "Simultaneous wireless information and power transfer (SWIPT): Recent advances and future challenges," *IEEE Commun. Surv. Tut.*, vol. 20, no. 1, pp. 264–302, Jan.–Mar. 2018, doi: 10.1109/COMST.2017.2783901.

[13] X. Yu, J. Feng, and Q. Li, "A planar omnidirectional wireless power transfer platform for portable devices," in *Proc. IEEE Appl. Power Electron. Conf. Expo.*, 2023, pp. 1654–1661, doi: 10.1109/APEC43580.2023.10131566.

[14] J. Feng, Q. Li, F. C. Lee, and M. Fu, "LCCL-LC resonant converter and its soft switching realization for omnidirectional wireless power transfer systems," *IEEE Trans. Power Electron.*, vol. 36, no. 4, pp. 3828–3839, Apr. 2021, doi: 10.1109/TPEL.2020.3024757.

[15] J. Feng, Q. Li, F. C. Lee, and M. Fu, "Transmitter coils design for free-positioning omnidirectional wireless power transfer system," *IEEE Trans. Ind. Inform.*, vol. 15, no. 8, pp. 4656–4664, Aug. 2019, doi: 10.1109/TII.2019.2908217.

[16] J. Kim, D.-H. Kim, J. Choi, K.-H. Kim, and Y.-J. Park, "Free-positioning wireless charging system for small electronic devices using a bowl-shaped transmitting coil," *IEEE Trans. Microw. Theory Techn.*, vol. 63, no. 3, pp. 791–800, Mar. 2015, doi: 10.1109/TMTT.2015.2398865.

[17] D. Lin, C. Zhang, and S. Y. R. Hui, "Mathematic analysis of omnidirectional wireless power transfer—Part-II three-dimensional systems," *IEEE Trans. Power Electron.*, vol. 32, no. 1, pp. 613–624, Jan. 2017, doi: 10.1109/TPEL.2016.2523506.

[18] X. Tian, K. T. Chau, W. Liu, H. Pang, and C. H. T. Lee, "Maximum power tracking for magnetic field editing-based omnidirectional wireless power transfer," *IEEE Trans. Power Electron.*, vol. 37, no. 10, pp. 12901–12912, Oct. 2022, doi: 10.1109/TPEL.2022.3178097.

[19] W. Han, K. T. Chau, C. Jiang, W. Liu, and W. H. Lam, "Design and analysis of quasi-omnidirectional dynamic wireless power transfer for fly-and-charge," *IEEE Trans. Magn.*, vol. 55, no. 7, Jul. 2019, Art. no. 8001709, doi: 10.1109/TMAG.2019.2895716.

[20] T. Feng, Z. Zuo, Y. Sun, X. Dai, X. Wu, and L. Zhu, "A reticulated planar transmitter using a three-dimensional rotating magnetic field for free-positioning omnidirectional wireless power transfer," *IEEE Trans. Power Electron.*, vol. 37, no. 8, pp. 9999–10015, Aug. 2022, doi: 10.1109/TPEL.2022.3155251.

[21] J. Lan, Y. Diao, X. Duan, and A. Hirata, "Planar omnidirectional wireless power transfer system based on novel metasurface," *IEEE Trans. Electromagn. Compat.*, vol. 64, no. 2, pp. 551–558, Apr. 2022, doi: 10.1109/TEMC.2021.3123047.

[22] B. H. Choi, E. S. Lee, Y. H. Sohn, G. C. Jang, and C. T. Rim, "Six degrees of freedom mobile inductive power transfer by crossed dipole Tx and rx coils," *IEEE Trans. Power Electron.*, vol. 31, no. 4, pp. 3252–3272, Apr. 2016, doi: 10.1109/TPEL.2015.2449290.

[23] T. Feng, Y. Sun, Y. Feng, and X. Dai, "A tripolar plane-type transmitter for three-dimensional omnidirectional wireless power transfer," *IEEE Trans. Ind. Appl.*, vol. 58, no. 1, pp. 1254–1267, Jan./Feb. 2022, doi: 10.1109/TIA.2021.3107471.

[24] Y. Zhang, C. Liu, M. Zhou, and X. Mao, "A novel asymmetrical quadrupolar coil for interoperability of unipolar, bipolar, and quadrupolar coils in electric vehicle wireless charging systems," *IEEE Trans. Ind. Electron.*, vol. 71, no. 4, pp. 4300–4303, Apr. 2024, doi: 10.1109/TIE.2023.3277123.

[25] P. Jayathurathnage, Y. Liu, and J. Kyyrä, "Self-decoupled and integrated coils for modular multitransmitter wireless power transfer systems," *IEEE Trans. Power Electron.*, vol. 37, no. 11, pp. 12962–12967, Nov. 2022, doi: 10.1109/TPEL.2022.3181508.

[26] H. Pang, K. T. Chau, W. Han, W. Liu, and Z. Zhang, "Decoupled-double D coils based dual-resonating-frequency compensation topology for wireless power transfer," *IEEE Trans. Magn.*, vol. 58, no. 2, Feb. 2022, Art. no. 8000407, doi: 10.1109/TMAG.2021.3091456.

[27] Y. Wang, A. Sun, F. Wang, and B. Liu, "Analysis and design of wireless bidirectional power and data transfer with decoupled DD-R coil geometry," *IEEE Trans. Transp. Electrific.*, early access, Sep. 26, 2023, doi: 10.1109/TTE.2023.3319507.

[28] H. Wang, K. W. E. Cheng, X. Li, and J. Hu, "A special magnetic coupler structure for three-coil wireless power transfer: Analysis, design, and experimental verification," *IEEE Trans. Magn.*, vol. 57, no. 11, Nov. 2021, Art. no. 8002108, doi: 10.1109/TMAG.2021.3111738.

[29] W. Pan, C. Liu, H. Tang, Y. Zhuang, and Y. Zhang, "An interoperable electric vehicle wireless charging system based on mutually spliced double-D coil," *IEEE Trans. Power Electron.*, vol. 39, no. 3, pp. 3864–3872, Mar. 2024, doi: 10.1109/TPEL.2023.3344663.

[30] F. W. Grover, *Inductance Calculations: Working Formulas and Tables*, Dover phoenix editions. Dover Publications: New York, NY, USA, 2004. [Online]. Available: https://books.google.com/books?id=K3KHi9lIltsC

[31] Y. Zhang, Z. Zhao, and K. Chen, "Frequency decrease analysis of resonant wireless power transfer," *IEEE Trans. Power Electron.*, vol. 29, no. 3, pp. 1058–1063, Mar. 2014, doi: 10.1109/TPEL.2013.2277783.

[32] R. Tseng, B. von Novak, S. Shevde, and K. A. Grajski, "Introduction to the alliance for wireless power loosely-coupled wireless power transfer system specification version 1.0," in *Proc. IEEE Wireless Power Transfer*, 2013, pp. 79–83, doi: 10.1109/WPT.2013.6556887.

[33] Y. Jiang et al., "A dynamic efficiency optimization method under ZVS conditions in the series-series type wireless power transfer system," in *Proc. IEEE Energy Convers. Congr. Expo.*, 2020, pp. 995–1001, doi: 10.1109/ECCE44975.2020.9235452.

[34] D. van Wageningen and T. Staring, "The Qi wireless power standard," in *Proc. 14th Int. Power Electron. Motion Control Conf.*, 2010, pp. S15-S25–S15-32, doi: 10.1109/EPEPEMC.2010.5606673.

[35] Y. Jiang et al., "Efficiency optimization of WPTS based on variable angle phase shift control for EV charging," in *Proc. IEEE 9th Int. Power Electron. Motion Control Conf.*, 2020, pp. 747–752, doi: 10.1109/IPEMC-ECCEAsia48364.2020.9368148.

[36] Y. Li et al., "A universal parameter design method of resonant coils under multiple boundary constrains for wireless power transfer systems," in *Proc. IEEE Energy Convers. Congr. Expo.*, 2023, pp. 6489–6496, doi: 10.1109/ECCE53617.2023.10362919.

[37] M. Budhia, J. T. Boys, G. A. Covic, and C.-Y. Huang, "Development of a single-sided flux magnetic coupler for electric vehicle IPT charging systems," *IEEE Trans. Ind. Electron.*, vol. 60, no. 1, pp. 318–328, Jan. 2013, doi: 10.1109/TIE.2011.2179274.

[38] H. Wang and K. W. E. Cheng, "Analysis, design, and validation of a decoupled double-receiver wireless power transfer system with constant voltage outputs for industrial power supplies," *IEEE Trans. Ind. Inf.*, vol. 19, no. 1, pp. 362–370, Jan. 2023, doi: 10.1109/TII.2022.3165248.